

# Informative Policy Representations in Multi-Agent Reinforcement Learning via Joint-Action Distributions

Yifan Yu<sup>\*</sup>, Haobin Jiang<sup>\*</sup>, Zongqing Lu<sup>†</sup>

Peking University  
{markyu, haobin.jiang, zongqing.lu}@pku.edu.cn

## Abstract

In multi-agent reinforcement learning, the inherent non-stationarity of the environment caused by other agents' actions posed significant difficulties for an agent to learn a good policy independently. One way to deal with non-stationarity is agent modeling, by which the agent takes into consideration the influence of other agents' policies. Most existing work relies on predicting other agents' actions or goals, or discriminating between their policies. However, such modeling fails to capture the similarities and differences between policies simultaneously and thus cannot provide useful information when generalizing to unseen policies. To address this, we propose a general method to learn representations of other agents' policies via the joint-action distributions sampled in interactions. The similarities and differences between policies are naturally captured by the policy distance inferred from the joint-action distributions and deliberately reflected in the learned representations. Agents conditioned on the policy representations can well generalize to unseen agents. We empirically demonstrate that our method outperforms existing work in multi-agent tasks when facing unseen agents.

## Introduction

In recent years, deep reinforcement learning (RL) achieved tremendous success in a range of complex tasks, such as Atari games (Mnih et al. 2015), Go (Silver et al. 2016, 2017), and StarCraft (Vinyals et al. 2019). However, real-world scenarios often require multiple agents instead of one. With the introduction of other agents, the environment is no longer stationary in the view of each individual agent in the multi-agent system, when the joint policy of other agents is changing. The non-stationary nature and the explosion of dimensions pose many challenges to learning in multi-agent environments.

To address these challenges, centralized and decentralized algorithms (Lowe et al. 2017; Zhang et al. 2018), communication (Foerster et al. 2016; Sukhbaatar, Fergus et al. 2016; Peng et al. 2017; Jiang and Lu 2018), value decomposition (Sunehag et al. 2018; Rashid et al. 2018; Foerster et al. 2018b; Son et al. 2019) and agent modeling (He et al. 2016; Hong et al. 2018; Raileanu et al. 2018) are proposed successively in attempts to improve the performance of deep RL

algorithms in various multi-agent settings, such as competition and cooperation, from different perspectives.

One way to address non-stationarity is to distinguish between the invariant dynamics of the environment and the influence of other agents' joint policy, and consider them separately in order to learn an effective policy. In this way, agent modeling has become one of the main research directions, in which the goals, policies or actions of other agents are predicted or represented as auxiliary tasks of the RL algorithms (He et al. 2016; Hong et al. 2018; Grover et al. 2018). Thus, the agent's decision takes into account the dynamics of the environment and other agents separately, leading to improved performance during training and execution.

In this paper, we focus on the multi-agent learning problem that one agent learns while interacting with other agents (collectively termed as *opponents* for convenience, whether collaborators or competitors), whose policies are sampled from a set of fixed policies at the beginning of each episode during training. To perform well, the learning agent should be able to distinguish different opponents' policies and adopt its corresponding policy. More importantly, we expect this agent to be immediately generalizable, *i.e.*, to adapt quickly and achieve high performance when facing unseen opponents during execution without updating parameters. Note that this setting is different from the continuous adaptation problem (Al-Shedivat et al. 2018; Foerster et al. 2018a; Kim et al. 2020), where both the agent and opponents learn continuously.

Similarity can be defined as the distance in physical space or in mental space (Shepard 1957), and plays an important role in problem solving, reasoning, social decision making, *etc.* (Hahn, Chater, and Richardson 2003). Some cognitive and social science theories suggest that the observer constructs mental representations for persons. When encountering a new person, the observer makes judgements and inferences based on the similarity between the new individual and known ones (Smith and Zarate 1992). Therefore, we believe it is also important to consider the similarity between different opponents' policies when modeling them, rather than mere distinction. Inspired by this theory, we propose *Informative Policy Representations* (IPR), a novel method to learn policy representations which are informative in that they reflect both similarities and differences by capturing the distances between different policies of opponents.

<sup>\*</sup>Equal contribution

<sup>†</sup>Correspondence to Zongqing Lu <zongqing.lu@pku.edu.cn>

In multi-agent tasks, the distance between different agent policies are naturally reflected in the difference between action patterns, and eventually in that of joint-action distributions that can be sampled in interactions with different policies. IPR exploits these distributions to quantify the policy-distance so as to essentially model the policy space, and embeds these information in the corresponding policy representations. In this way, IPR can accomplish quick adaptation and generalization no matter in competitive or cooperative, partially or fully observable settings. Through experiments, we demonstrate that IPR can greatly improve the learning of existing RL algorithms, especially when interacting with opponents with unseen policies. We further show that the learned policy representations correctly reflect the relations between policies.

## Related Work

In the continuous adaptation problem, the change of opponents’ policies comes from the parameter update. LOLA (Foerster et al. 2018a) takes opponents’ learning process into consideration, where the agent acquires high rewards by shaping the learning directions of the opponents. Al-Shedivat *et al.* [2018] proposed a method based on meta policy gradient and Kim *et al.* [2020] extends this method by introducing the opponent learning gradient.

Unlike continuous adaptation, in settings like ours where the opponents act based on fixed policies, direct modeling of opponents becomes effective. One approach is to predict actions or goals of opponents via deep neural networks, which serves as an auxiliary task for RL. Based on DQN (Mnih et al. 2015), DRON (He et al. 2016) and DPIQN (Hong et al. 2018) use a secondary network which takes observations as inputs and predicts opponents’ actions. The hidden layer of this network is used by the DQN module to condition on for better policy. DRON and DPIQN are trained using the RL loss and the loss of the auxiliary task simultaneously. SOM (Raileanu et al. 2018) uses its own policy to estimate the goals of opponents, behaving like human’s Theory of Mind (Premack and Woodruff 1978).

Representation learning is also explored for agent modeling. These methods usually use an encoder mapping observations to the representation space. Grover *et al.* [2018] learns policy representation to model and distinguish agents’ policies by predicting their actions and identifying them through triplet loss. In fact, the auxiliary tasks in DRON (He et al. 2016) and DPIQN (Hong et al. 2018) can also be viewed essentially as representation learning.

Though having achieved high performance in multi-agent tasks, many of the aforementioned methods have limitations or do not specifically consider generalization in execution. SOM (Raileanu et al. 2018) and DRON (He et al. 2016) require opponents’ observations or actions to do inference, which may be unrealistic in execution. DPIQN (Hong et al. 2018) and Grover *et al.* [2018] do use local information only.

However, training with action prediction as a supervision signal makes the performance rely heavily on the unseen policy to be similar enough to training policies. Moreover, Grover *et al.* [2018] captures only differences between op-

ponents’ policies, but ignores similarities that we believe are important.

Our proposed IPR avoids these deficiencies by learning representations that reflect distances between opponents’ policies, capturing both similarities and differences between them. Thus, IPR essentially models the policy space, so that it adapts immediately when facing unseen policies in execution without parameter updating like continuous learning (Al-Shedivat et al. 2018; Kim et al. 2020). Besides, the agent requires no additional information other than its own observations during execution.

## Preliminaries

### Multi-Agent Environment

We use a setting similar to Hong *et al.* [2018] to model a multi-agent environment  $\mathcal{E}$  with  $N + 1$  independent agents: one learning agent and the other  $N$  agents with any policies. At each timestep, the learning agent selects an action  $a \in \mathcal{A}$ , while the other  $N$  agents’ actions form a joint action  $\mathbf{a}_o \in \mathcal{A}_o$ , where  $\mathcal{A}_o = \mathcal{A}_1 \times \mathcal{A}_2 \times \dots \times \mathcal{A}_N$ . The subscript  $o$  denotes “opponents”, and  $\mathcal{A}_1, \dots, \mathcal{A}_N$  corresponds to each of the  $N$  agents’ action space. The policies of the  $N$  agents form a joint policy denoted by  $\pi_o(\mathbf{a}_o|o_o)$ , where  $o_o$  denotes the joint observation of the  $N$  agents. The policy of each of the  $N$  agents is consistent within the same episode. We define the learning agent’s policy as  $\pi(a|o, \pi_o)$  to condition on  $\pi_o$ . We make no assumptions on agents’ relations with each other: each pair of agents in  $\mathcal{E}$  can be either collaborators or competitors. The reward of the learning agent at each timestep is given by a reward function  $\mathcal{R}: r = \mathcal{R}(s, a, \mathbf{a}_o, s')$ , and the state transition function is  $\mathcal{T}(s', s, a, \mathbf{a}_o) = \Pr(s'|s, a, \mathbf{a}_o)$ .

### Agent’s Policy Space

We notice the number of different possible policies that each of the other agents can take is numerous, *if not infinite*. For generalization to any possible policies, we consider the “policy space”  $\Pi_i$  formed by all possible policies of agent  $i$  in  $\mathcal{E}$ . In each episode, agent  $i$  acts according to a policy  $\pi_i$  which is sampled from a distribution  $P_i$  over  $\Pi_i$ . Therefore, the joint policy of the  $N$  agents  $\pi_o$  can be viewed as sampled from the joint distribution  $\mathbf{P}$  over the joint policy space  $\Pi_o : \Pi_1 \times \Pi_2 \times \dots \times \Pi_N$ .

### The Multi-Agent Learning Problem

In this paper, we focus on the learning problem for the *learning agent* described as follows. Given environment  $\mathcal{E}$  with  $N + 1$  agents, a training policy set  $\Pi_o^{\text{train}} = \Pi_1^{\text{train}} \times \Pi_2^{\text{train}} \times \dots \times \Pi_N^{\text{train}}$  resembles the distribution  $\mathbf{P}$  over  $\Pi_o$ , where each  $\Pi_i^{\text{train}}$  resembles the distribution  $P_i$  over  $\Pi_i$ . In each episode during training, the learning agent interacts with the other  $N$  agents with policy  $\pi_1 \in \Pi_1^{\text{train}}, \pi_2 \in \Pi_2^{\text{train}}, \dots, \pi_N \in \Pi_N^{\text{train}}$ , respectively. These policies form a joint policy  $\pi_o^{\text{train}} \in \Pi_o^{\text{train}}$ , on which the learning agent should condition its policy to maximize the expected return. The learning agent is tested against agents with joint policy  $\pi_o^{\text{test}}$  from the test policy set, where  $\Pi_o^{\text{test}} = \Pi_1^{\text{test}} \times \Pi_2^{\text{test}} \times \dots \times \Pi_N^{\text{test}}$  and  $\Pi_o^{\text{test}} \cap \Pi_o^{\text{train}} = \emptyset$ . During test, the learning

agent has to not only discriminate different (joint) policies in  $\Pi_o$  to condition its own policy, but also calibrate the distances between policies through their representations, and thus achieve high return when facing unseen policies. Once again, we assume the learning agent do not update the policy during test, which is different from meta-learning methods, like MAML (Finn, Abbeel, and Levine 2017).

## Method

Firstly, we estimate the distances between opponents’ (joint) policies by the distances between the sampled joint-action distributions. IPR then uses the estimated policy-distances to train an encoder network so that the obtained representation-distances correctly reflect the distances between opponents’ policies. As a general framework, IPR can function with any RL algorithms as an auxiliary module, providing informative representation of opponents’ (joint) policy.

### Policy-Distance Estimation via Joint-Action Distributions

Intuitively, the distances between policies are naturally reflected in the differences of respective action patterns. From the learning agent’s perspective, fixing its own policy and exploration, the different (joint) policies of opponents can be captured in the different distributions of  $(a, \mathbf{a}_o, s)$  in interactions. However, it is impractical to iterate over all possible tuples and collect enough samples to estimate the distribution of  $(a, \mathbf{a}_o, s)$ , given a large state space or continuous action space. Instead, we propose to use the differences in the sampled distributions of  $(a, \mathbf{a}_o)$  in interactions with different (joint) policies as an approximate estimate of the distances between these policies. Given sufficient samples, the sampled frequency of  $(a, \mathbf{a}_o)$  can be used as an approximation to the actual  $\mathbb{E}_s [p(a, \mathbf{a}_o)]$  which is the expected probability of  $(a, \mathbf{a}_o)$  over all states. As we will show in Figure 6, this gives a good enough measurement to estimate the policy-distance. Concretely, we fix the learning agent’s own policy and exploration for sampling. The corresponding samples of  $(a, \mathbf{a}_o)$  are taken by interacting with each  $\pi_o^i$  in training policy set  $\Pi_o^{\text{train}}$  in the environment  $\mathcal{E}$ .

For an environment  $\mathcal{E}$  with discrete action spaces, in which  $\mathcal{A}, \mathcal{A}_1, \dots, \mathcal{A}_N$  are all discrete spaces, we calculate the frequency distribution  $f^i$  of all possible pairs of  $(a, \mathbf{a}_o)$  using the samples taken with  $\pi_o^i$  as an estimate of the real probability distribution  $p^i$ . Then we use the Kullback-Leibler (KL) divergence between these distributions as a measure for the distance between the policies  $\pi_o^i$  and  $\pi_o^j$ ,

$$\begin{aligned} d(\pi_o^i, \pi_o^j) &= D_{\text{KL}}(p^i || p^j) + D_{\text{KL}}(p^j || p^i) \\ &\approx D_{\text{KL}}(f^i || f^j) + D_{\text{KL}}(f^j || f^i). \end{aligned} \quad (1)$$

For an environment with continuous action space, in which at least one of  $\mathcal{A}, \mathcal{A}_1, \dots, \mathcal{A}_N$  is continual, we propose to use Wasserstein distance as a measurement for the distance between  $\pi_o^i$  and  $\pi_o^j$ . The reason for using Wasserstein distance is that the sampled data points can be used to compute the distance directly without estimating the empirical distributions of samples, which is intractable in contin-



Figure 1: Intuitive illustration of policy representations reflecting their relations in policy space.

uous action space,

$$d(\pi_o^i, \pi_o^j) = W(p^i, p^j) \approx W(y^i, y^j) \quad (2)$$

where  $y^i$  is the set of  $(a, \mathbf{a}_o)$  samples taken with  $\pi_o^i$ . While computationally demanding in high-dimensional space, the Wasserstein distance in one-dimensional space can be computed easily. So an alternative metric, sliced Wasserstein distance (Rabin et al. 2011), is used to approximate the Wasserstein distance, which is obtained by projecting the raw  $m$ -dimensional data points into one-dimensional space and computing one-dimensional Wasserstein distance,

$$SW(X, Y) = \int_{\sigma \in \mathbb{S}^{m-1}} W(\sigma^T X, \sigma^T Y) d\sigma \quad (3)$$

where  $\mathbb{S}^{m-1}$  is the unit sphere in  $m$ -dimensional space. In practice, the sliced Wasserstein distance is usually approximated by summation over randomly projections (Deshpande, Zhang, and Schwing 2018),

$$\tilde{SW}(X, Y) = \frac{1}{|\Omega|} \sum_{\sigma \in \Omega} W(\sigma^T X, \sigma^T Y) \quad (4)$$

where  $\Omega$  is the set of randomly generated projections. We use the approximated sliced Wasserstein distance in practice to reduce the computational overhead.

### Informative Representations Learning based on Policy-Distance

Inspired by the theory on similarity and optimization objective setting in Ghosh *et al.* [2019], IPR tries to learn informative representations that reflect the distances between policies, thus can well generalize to unseen policy with a good estimate of its relations to known policies using the policy-distance measure. Such representations are generated through an encoder network  $\phi$  parameterized by  $\theta$ , minimizing the following loss function  $\mathcal{L}_{\text{embed}}$ :

$$\mathcal{L}_{\text{embed}}(\theta) = \mathbb{E}_{\pi_o^i, \pi_o^j \sim \Pi_o^{\text{train}}} \left[ \left( \text{Dist}(\phi(\pi_o^i; \theta), \phi(\pi_o^j; \theta)) - d(\pi_o^i, \pi_o^j) \right)^2 \right]. \quad (5)$$

$\text{Dist}(\cdot, \cdot)$  is a distance function between two output representations of  $\phi$  network (*e.g.*, L2 distance). The *rhs* of (5) optimizes the encoder network  $\phi$  such that the distance between the representations of each pair of  $\pi_o^i$  and  $\pi_o^j$  converges to  $d(\pi_o^i, \pi_o^j)$ .

Intuitively, for an agent in a certain environment where its policy can be offensive, defensive or halfway in the middle (50-50), the policy representations that we try to learn

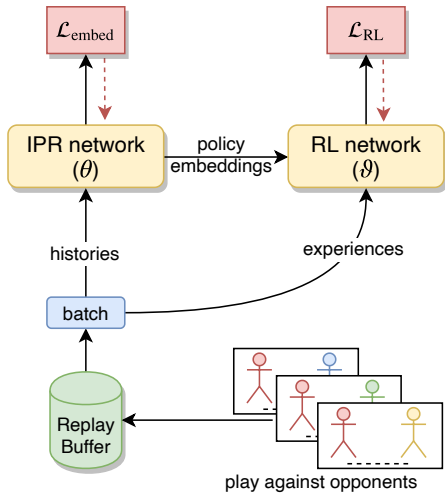


Figure 2: Illustration of IPR with RL framework.

here, of this agent, should be able to visualized as Figure 1. The policy representations should be able to not only distinguish different policies (*i.e.*, the representations of same policy gather in clusters while separate from others), but also capture their relative positions in the policy space (*i.e.*, placing the 50-50 policy in the middle of the other two).

In training, we use the L2 distance as the Dist function. The encoder network is learned in a supervised way. At each timestep  $t$ , we takes a history concatenated by past observations of the learning agent  $\mathbf{h}_t = \langle o_0, o_1, \dots, o_{t-1}, o_t \rangle$  and the label  $i$  of the policy  $\pi_o$  the agent is facing in that episode, and store the pair  $\langle \mathbf{h}^i, i \rangle$  into a buffer  $\mathcal{B}$ .

Each training batch is uniformly sampled from the buffer and hence the encoder network is optimized by

$$\mathcal{L}_{\text{embed}}(\theta) = \mathbb{E}_{\langle \mathbf{h}^i, i \rangle, \langle \mathbf{h}^j, j \rangle \sim \mathcal{B}} \left[ \left( \left\| \phi(\mathbf{h}^i; \theta) - \phi(\mathbf{h}^j; \theta) \right\| - d(\pi_o^i, \pi_o^j) \right)^2 \right]. \quad (6)$$

### Informative Policy Representations with RL Algorithm

Figure 2 illustrates a general framework that combines IPR with RL algorithms. The histories and experiences are stored together in the replay buffer. The IPR network  $\phi(\mathbf{h}; \theta)$ , *i.e.* the encoder network described above, takes histories from replay buffer as input to generate representations of opponents' (joint) policies in the corresponding episodes, and optimizes its parameters  $\theta$  to minimize  $\mathcal{L}_{\text{embed}}$ . The output representation (current opponents' joint policy embedding) of the IPR network, generated by taking as input the history so far in current episode, is fed into the RL network as an additional input, making the learning agent's policy condition on opponents' policies  $\pi_o$  approximately. The RL module optimizes its parameters  $\vartheta$  to minimize its own loss  $\mathcal{L}_{\text{RL}}$  conditioned on the representations.

The training process is described in Algorithm 1. The empirical joint-action distribution can be sampled by using a random policy against opponents at the beginning of

---

### Algorithm 1 Joint Training of IPR and RL

---

**Require:** Training policy set  $\Pi_o^{\text{train}} = \{\pi_o^1, \pi_o^2, \dots, \pi_o^N\}$

- 1: Initialize  $\mathcal{E}$ , replay buffer  $\mathcal{B}$ , IPR network parameters  $\theta$ , RL network parameters  $\vartheta$
  - 2: Initialize joint-action distributions  $\mathcal{D}_1, \mathcal{D}_2, \dots, \mathcal{D}_N$
  - 3: **for**  $\pi_o^k \in \Pi_o^{\text{train}}$  **do**
  - 4:   **for**  $n = 1$  to  $\text{num\_sample\_episodes}$  **do**
  - 5:     Reset  $\mathcal{E}$  with other agents' policy set to  $\pi_o^k$
  - 6:     Roll out one episode  $e$  using random policy
  - 7:     Update  $\mathcal{D}_k$  with all  $(a, \mathbf{a}_o)$  pairs from  $e$
  - 8:     Store  $\langle \mathbf{h}, k, o, a, r, o' \rangle$  of  $e$  in  $\mathcal{B}$
  - 9:   **end for**
  - 10: **end for**
  - 11: Calculate  $d(\pi_o^i, \pi_o^j)$  for all  $(i, j)$  using  $\mathcal{D}_i, \mathcal{D}_j$
  - 12: **for** training step  $t = 1$  to  $T$  **do**
  - 13:   Sample a batch from  $\mathcal{B}$
  - 14:   Update  $\theta$  by  $\mathcal{L}_{\text{embed}}(\theta)$
  - 15:   Update  $\vartheta$  by  $\mathcal{L}_{\text{RL}}(\vartheta)$
  - 16:   **if**  $t \bmod \text{play\_frequency} = 0$  **then**
  - 17:     Reset  $\mathcal{E}$  and clear history  $\mathbf{h} \leftarrow \emptyset$  if necessary
  - 18:     Rollout  $\text{play\_step}$  steps using  $\pi(a|o, \phi(\mathbf{h}; \theta); \vartheta)$
  - 19:     Store  $\langle \mathbf{h}, k, o, a, r, o' \rangle$  in  $\mathcal{B}$
  - 20:   **end if**
  - 21:   **if** IPR-RS **AND**  $t \bmod \text{resample\_period} = 0$  **then**
  - 22:     Re-Sample  $\mathcal{D}_1, \mathcal{D}_2, \dots, \mathcal{D}_N$
  - 23:     Calculate  $d(\pi_o^i, \pi_o^j)$  for all  $(i, j)$  using  $\mathcal{D}_i, \mathcal{D}_j$
  - 24:   **end if**
  - 25: **end for**
- 

the training, or by periodically sampling along with training. The periodic re-sampling can be taken based on current policy or from replay buffer. Two options differ in Algorithm 1 on whether lines 21-24 are executed periodically, and denoted as IPR-NoRS and IPR-RS (where RS stands for *Re-Sample*), respectively. In practice, as we will show in experiments, the choice of the two is made based on the environment settings and experimental results because of their different pros and cons. IPR-RS continues to obtain current joint-action distributions under the learning agent's updated policy, but also produces moving targets for  $\mathcal{L}_{\text{embed}}$ . IPR-NoRS has a fixed optimization target for better convergence, but the calculated distances might not give an useful estimation in later period of training.

Note that our method does not require perfect information of opponents' (joint) policies. Only opponents' actions  $\mathbf{a}_o$  and their labels  $i$  are required for obtaining the joint-action distributions and estimating policy-distances during training. In execution, only local observed history  $\mathbf{h}$  are needed to generate a good policy against diverse opponents, which is practical in most scenarios.

Our method allows for some scalability. The increase in the number of opponents' policies only affects the time to estimate policy-distances. After the policy-distances have been calculated, the policy-distance between each pair of opponent policies can be retrieved directly as from a look-up table, thus the number of opponents' policies has almost no additional cost. As for the estimation time of policy-distances, KL-divergence is fast to calculate from the sampled frequency distributions. Approximated sliced Wasserstein distance may take longer, but in IPR-NoRS it only

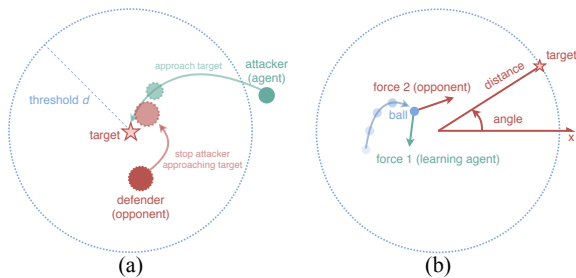


Figure 3: Illustration of (a) Push, (b) Keep.

needs to be calculated once, where the estimation time is insignificant compared to the overall training time.

## Experiments

We evaluate our method’s performance in two multi-agent environments: *Push* with discrete action space and *Keep* with continuous action space. The former is partially observable, while the latter is fully observable.

### Push

**Task and Setting** Our *Push* environment is modified based on the original *simple-push* scenario of Multi-Agent Particle Environment (Mordatch and Abbeel 2018; Lowe et al. 2017). As shown in Figure 3(a), *Push* contains no borders, one landmark (“*target*”) fixed at origin  $(0, 0)$ , and two competitive agents—a learning agent (“*attacker*”) which tries to approach and touch the *target*, and a defensive opponent (“*defender*”) which tries to stop the *attacker* from approaching the *target* and push it away. Each agent has a discrete action space consists of 5 actions and corresponds to applying a zero force, or a unit force on four directions. The *defender* has a larger size and mass but a smaller acceleration and maximum velocity than the *attacker*. Each timestep, the *attacker* receives a negative reward of its distance to the landmark,  $+2$  reward if it touches the landmark, and  $-2$  reward if it is collided with the *defender*. The learning agent’s observation at each timestep consists of the agent’s relative positions with *target* and *defender*, and its own velocity. The opponent’s velocity is unknown to the learning agent, thus making *Push* partially observable. The *defender*’s policy is set with scripted rule-based policy. Each timestep, the *defender* calculates the *attacker*’s distance to the *target* using its observation. If the distance is larger than a threshold parameter  $d$ , the *defender* moves towards the *target*, otherwise it moves towards the *attacker*. Its output action is a unit force on the direction towards its current target. The maximum timestep in each episode is set to 50.

In this experiment, the training policy set consists of 4 different policies with different threshold parameter  $d$  for the *defender*:  $d = 0.1, 0.3, 0.75, 1.0$ . The testing policy is set with  $d = 0.5$ . We combined our IPR method with DQN (Mnih et al. 2015), and compared the performance when interacting with the test opponent of our method (DQN+IPR-NoRS and DQN+IPR-RS) with DPIQN (Hong et al. 2018) which uses the same architecture as DQN+IPR but trains

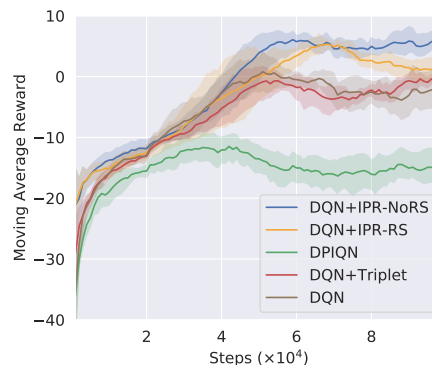


Figure 4: Moving average of test rewards in *Push*. The moving average is taken by the mean of recent 20 tests, one per each 1000 training steps. Each curve corresponds to the mean value of 5 trials with different random seeds, and shaded regions indicate 95% CI.

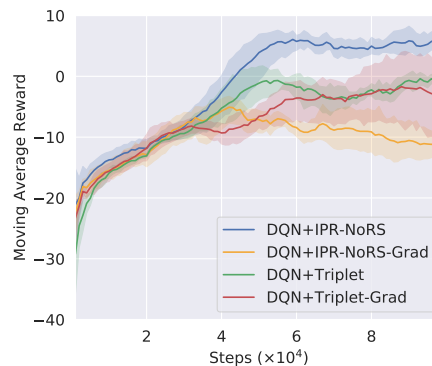


Figure 5: Moving average of test rewards in *Push*. The versions with RL loss gradients back-propagated to encoders are denoted with additional suffix “*Grad*” to the original methods.

the IPR network with cross-entropy loss to predict the opponents’ actions and with RL loss gradients back-propagated to the encoder, DQN+Triplet which uses the same architecture as DQN+IPR but trains the IPR network with triplet loss that resembles Grover *et al.* [2018] and only distinguishes between different opponents’ policies, and vanilla DQN without the encoder network of IPR. More details about the networks and hyperparameters are available in Appendix.

**Quantitative Results** Figure 4 shows the moving average reward when testing against the test policy ( $d = 0.5$ ) of our method and the baselines. The tests are run every 1000 steps during training, and the moving average reward is taken by the mean of recent 20 tests. As the result shows, DQN+IPR-NoRS and DQN+IPR-RS outperform the compared methods when facing the unseen policy, thus proving the effectiveness of our proposed method. IPR-NoRS performs slightly better than IPR-RS in this environment, which might be the result of the moving target problem and also of the learned policy limits the re-sampling from capturing as much infor-



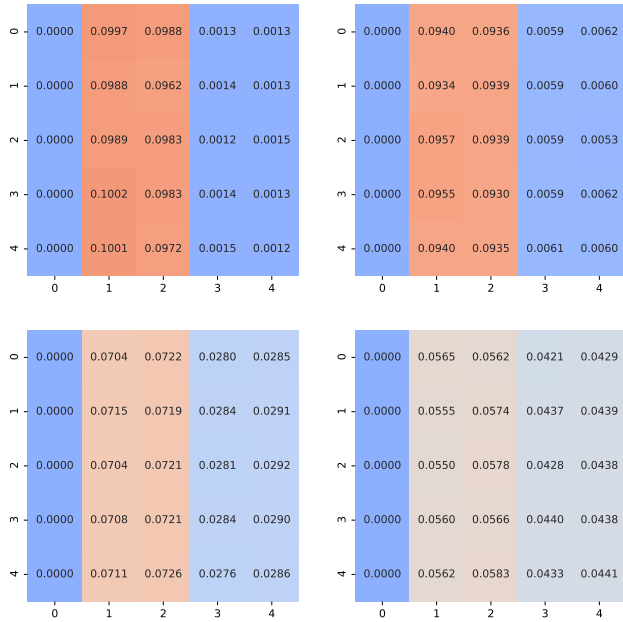


Figure 6: Heatmaps of the initial sampling results against the four training opponent policies under one random seed in Push, where x-axis indicates the opponent’s action and y-axis the (random) agent’s. Colors and values indicate the frequency of the corresponding joint-action pairs. Action 0 exerts zero force, and actions 1-4 each exerts unit force towards one of the four directions.

mation of different policies as random sampling.

Regarding the other compared methods, we infer that because of the threshold settings, DPIQN can hardly learn useful predictions on opponent’s actions through observed history, from which can hardly deduce which of the two acting patterns the opponent will act on. DQN essentially views the different policies as one, and triplet loss maximizes the difference between policy representations regardless of their relations. Thus all compared methods perform worse than IPR.

In the results above, the IPR methods (DQN+IPR-NoRS and DQN+IPR-RS) and DQN+Triplet method do not back-propagate RL loss gradients to the encoders. This choice is based on experimental results showing that doing such back-propagation significantly harms the performance of these methods, as shown in Figure 5. The suffix “*Grad*” corresponds to the versions that the RL loss gradients are back-propagated to encoders. We infer that the gradients from RL loss will interfere with the encoder’s embedding loss to make it hard to learn useful embeddings of the opponent policies, causing the decrease in test reward and increase in variance.

**Empirical Joint-Action Distribution** As described in Method, we empirically use the sampled frequency of  $(a, \mathbf{a}_o)$  as an approximation to the actual  $\mathbb{E}_s [p(a, \mathbf{a}_o)]$ . Figure 6 illustrates this estimation. The four heatmaps show the initial sampling results using random policy against the four training opponent policies  $d = 0.1, 0.3, 0.75, 1.0$  in order,

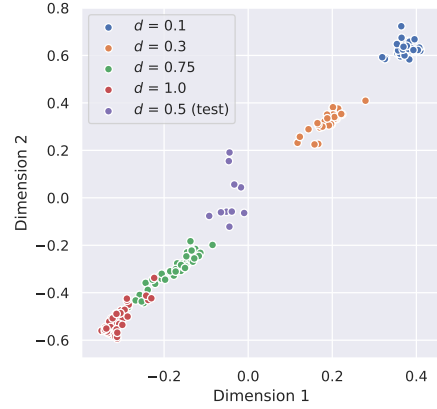


Figure 7: Opponent policy embeddings generated by IPR network in last 10 timesteps in an episode on Push. Dimension reduced by multidimensional scaling (MDS) to 2.

and the colors and values on each square of the heatmaps indicate the frequency of the corresponding joint-action pair composed by the agent’s action (y-axis) and the opponent’s (x-axis). It is easy to see that the frequency of every joint-action pair (except for the opponent taking 0) increases or decreases monotonically across the four heatmaps, which corresponds to the orderly change of the parameter  $d$ . This monotonic change is essentially caused by the different distributions  $p(a, \mathbf{a}_o)$  under different opponent policies. When  $d = 1.0$ , the opponent is more aggressive and chases after the learning agent everywhere, while when  $d = 0.1$ , the opponent stays around the origin for the most time. The different acting patterns cause the difference in  $p(a, \mathbf{a}_o)$  that is reflected in  $(a, \mathbf{a}_o)$  frequencies, thus allow our sampling to have a good estimation.

**Visualization of Learned Embeddings** In Figure 7, we visualize the learned policy embeddings (dimension reduced by MDS from 32 to 2) output by the encoder of one learned DQN+IPR-NoRS model on Push. The training policy embeddings ( $d = 0.1, 0.3, 0.75, 1.0$ ) are generated by the IPR encoder network from histories that are randomly taken from the final replay buffer. The test policy embeddings ( $d = 0.5$ ) are generated in actual test. Each shown embeddings correspond to one of the last 10 timesteps in an episode. The result shows that the learned embedding, including training and testing policies, can reflect to their relations (essentially the relations between different  $d$ ), thus validate our method’s hypothesis of policy embeddings reflecting the policy space, resemble the expected result in Figure 1.

## Keep

**Task and Setting** In order to verify the effectiveness of our method in continuous action space, we implement a simple two-agent environment named Keep. At the beginning of each episode, a ball is initialized around the origin  $(0, 0)$ . As illustrated in Figure 3(b), the learning agent tries to keep the ball close to the origin, while the opponent tries to pull the ball away from the origin. The opponent’s policy can be described as a triple  $(angle, distance, force)$ . For example,  $(45.0, 1.0, 0.5)$  means that the *target* is located at a dis-

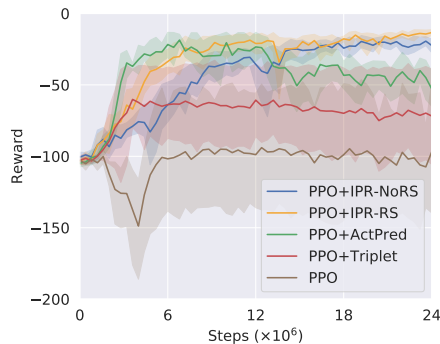


Figure 8: Average rewards against random testing opponent on `Keep`. At each checkpoint, rewards are averaged over 100 episodes. Each curve shows the mean value of 5 trials with different random seeds, and shaded regions indicate 95% CI.

tance of 1.0 from the origin and its angle from the x-axis is 45 degrees, same as polar coordinate, and the opponent will pull the ball towards the target with a force of 0.5. To make the task not too easy, we add some noise to the opponent’s action. The agent’s observation includes the coordinate and velocity of the ball, and the action is the magnitude and direction of the force exerted on the ball. Each timestep, the learning agent receives a negative reward of the distance between the ball and the origin. The length of each episode is set to 200.

In this experiment, the training policy set contains 4 different opponent policies:  $(45.0, 1.0, 0.5)$ ,  $(170.0, 2.0, 1.0)$ ,  $(-90.0, 1.5, 0.7)$ , and  $(0.0, 1.0, 0.3)$ . In test phase, the opponent policy is generated randomly at the beginning of each episode, where the ranges of angle, distance and force are  $[-180, 180)$ ,  $[0, 1)$  and  $[0.2, 1.7)$ , respectively.

Considering the continuous action space, the RL algorithm we choose to combine with IPR is Proximal Policy Optimization (PPO) (Schulman et al. 2017). Because the updates of policy network and value network are not simultaneous, we set separate IPR networks for them. As mentioned before, the difference between two opponent policies is estimated by the sliced Wasserstein distance between two sets of joint-action samples. A more detailed description of PPO+IPR will be given in Appendix. We compare our method (PPO+IPR-NoRS and PPO+IPR-RS) with PPO+ActPred (training the IPR network by predicting opponents’ actions, like DPIQN), PPO+Triplet (like (Grover et al. 2018)), and vanilla PPO without the encoder network. No gradients from policy network or value network are back-propagated to the IPR module.

**Quantitative Results** Figure 8 shows the average reward against the random testing opponent throughout training phase. The result suggests that PPO+IPR-NoRS and PPO+IPR-RS greatly outperform other methods. Although PPO+ActPred achieves almost the same reward as the former two early in the training, it shows high variance and its reward declines with training. PPO+IPR-NoRS and PPO+IPR-RS are more stable and continuously improve in the later stage of training, which implies our method’s effec-

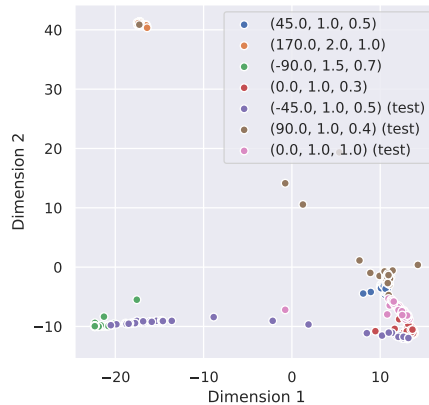


Figure 9: Opponent policy embeddings generated by IPR network on `Keep`, including four training opponents and three unseen test opponents. Dimension reduced by MDS to 2.

tiveness and better generalization to unseen opponents also in continuous action space. In addition, IPR-RS performs slightly better than IPR-NoRS in this environment, possibly because the initial sampling has interference from action pairs that sampled when the ball is far from the origin, while the later learned policy avoids such interference so different opponents’ policies show more individual characteristics.

**Visualization of Learned Embeddings** To demonstrate the interpretability of the embedding learned by PPO+IPR-RS on `Keep`, we select three unseen opponents for test:  $(-45.0, 1.0, 0.5)$ ,  $(90.0, 1.0, 0.4)$  and  $(0.0, 1.0, 1.0)$ . MDS on the embeddings is shown as Figure 9. Each point represents the average embedding over one episode. Among training opponent policies, the distance between the embeddings of  $(45.0, 1.0, 0.5)$  and  $(0.0, 1.0, 0.3)$  is the smallest, because their *angle* parameters are the closest. As for unseen opponents, we can see the embeddings of  $(-45.0, 1.0, 0.5)$  are located near  $(-90.0, 1.5, 0.7)$  and  $(0.0, 1.0, 0.3)$ , which is consistent with the physical meaning that  $-45.0$  is greater than  $-90.0$  but less than  $0.0$  and  $0.5$  is less than  $0.7$  but greater than  $0.3$ , even though the learning agent has not met  $(-45.0, 1.0, 0.5)$  during training. Other meaningful points include the embeddings of  $(0.0, 1.0, 1.0)$  are quite close to  $(0.0, 1.0, 0.3)$ , and  $(90.0, 1.0, 0.4)$  are near  $(45.0, 1.0, 0.5)$  and  $(170, 2.0, 1.0)$ .

## Conclusion

In this paper, we propose a general framework that learns informative policy representations that capture both the similarities and differences of other agents’ policies via joint-action distributions in multi-agent scenarios. Combining with existing RL algorithms, the policy takes actions conditioned on the learned policy representations of other agents. Through experiments, we demonstrate that the proposed framework can generalize better to unseen policies than existing methods, and the visualizations of the learned policy embeddings verify they can reflect the relations between policies in the policy space.

## References

- Al-Shedivat, M.; Bansal, T.; Burda, Y.; Sutskever, I.; Mordatch, I.; and Abbeel, P. 2018. Continuous adaptation via meta-learning in nonstationary and competitive environments. In *ICLR*.
- Deshpande, I.; Zhang, Z.; and Schwing, A. G. 2018. Generative Modeling Using the Sliced Wasserstein Distance. In *CVPR*.
- Finn, C.; Abbeel, P.; and Levine, S. 2017. Model-agnostic meta-learning for fast adaptation of deep networks. In *ICML*.
- Foerster, J.; Assael, I. A.; De Freitas, N.; and Whiteson, S. 2016. Learning to communicate with deep multi-agent reinforcement learning. In *NeurIPS*.
- Foerster, J.; Chen, R. Y.; Al-Shedivat, M.; Whiteson, S.; Abbeel, P.; and Mordatch, I. 2018a. Learning with opponent-learning awareness. In *AAMAS*.
- Foerster, J.; Farquhar, G.; Afouras, T.; Nardelli, N.; and Whiteson, S. 2018b. Counterfactual multi-agent policy gradients. In *AAAI*.
- Ghosh, D.; Gupta, A.; and Levine, S. 2019. Learning Actionable Representations with Goal Conditioned Policies. In *ICLR*.
- Grover, A.; Al-Shedivat, M.; Gupta, J. K.; Burda, Y.; and Edwards, H. 2018. Learning Policy Representations in Multiagent Systems. In *ICML*.
- Hahn, U.; Chater, N.; and Richardson, L. B. 2003. Similarity as transformation. *Cognition* 87(1): 1 – 32.
- He, H.; Boyd-Graber, J.; Kwok, K.; and Daumé III, H. 2016. Opponent modeling in deep reinforcement learning. In *ICML*.
- Hong, Z.-W.; Su, S.-Y.; Shann, T.-Y.; Chang, Y.-H.; and Lee, C.-Y. 2018. A deep policy inference q-network for multi-agent systems. In *AAMAS*.
- Jiang, J.; and Lu, Z. 2018. Learning attentional communication for multi-agent cooperation. In *NeurIPS*.
- Kim, D.-K.; Liu, M.; Riemer, M.; Sun, C.; Abdulhai, M.; Habibi, G.; Lopez-Cot, S.; Tesauro, G.; and How, J. P. 2020. A Policy Gradient Algorithm for Learning to Learn in Multiagent Reinforcement Learning. *arXiv:2011.00382* .
- Lowe, R.; Wu, Y.; Tamar, A.; Harb, J.; Abbeel, P.; and Mordatch, I. 2017. Multi-Agent Actor-Critic for Mixed Cooperative-Competitive Environments. In *NeurIPS*.
- Mnih, V.; Kavukcuoglu, K.; Silver, D.; Rusu, A. A.; Veness, J.; Bellemare, M. G.; Graves, A.; Riedmiller, M.; Fidjeland, A. K.; Ostrovski, G.; et al. 2015. Human-level control through deep reinforcement learning. *Nature* 518(7540): 529–533.
- Mordatch, I.; and Abbeel, P. 2018. Emergence of Grounded Compositional Language in Multi-Agent Populations. In *AAAI*.
- Peng, P.; Yuan, Q.; Wen, Y.; Yang, Y.; Tang, Z.; Long, H.; and Wang, J. 2017. Multiagent bidirectionally-coordinated nets for learning to play starcraft combat games. *arXiv:1703.10069* .
- Premack, D.; and Woodruff, G. 1978. Does the chimpanzee have a theory of mind? *Behavioral and brain sciences* 1(4): 515–526.
- Rabin, J.; Peyré, G.; Delon, J.; and Bernot, M. 2011. Wasserstein Barycenter and Its Application to Texture Mixing. In *International Conference on Scale Space & Variational Methods in Computer Vision*.
- Raileanu, R.; Denton, E.; Szlam, A.; and Fergus, R. 2018. Modeling Others using Oneself in Multi-Agent Reinforcement Learning. In *ICML*.
- Rashid, T.; Samvelyan, M.; De Witt, C. S.; Farquhar, G.; Foerster, J.; and Whiteson, S. 2018. QMIX: Monotonic value function factorisation for deep multi-agent reinforcement learning. In *ICML*.
- Schulman, J.; Wolski, F.; Dhariwal, P.; Radford, A.; and Klimov, O. 2017. Proximal Policy Optimization Algorithms. *arXiv:1707.06347* .
- Shepard, R. N. 1957. Stimulus and response generalization: A stochastic model relating generalization to distance in psychological space. *Psychometrika* 22(4): 325–345.
- Silver, D.; Huang, A.; Maddison, C. J.; Guez, A.; Sifre, L.; Van Den Driessche, G.; Schrittwieser, J.; Antonoglou, I.; Panneershelvam, V.; Lanctot, M.; et al. 2016. Mastering the game of Go with deep neural networks and tree search. *Nature* 529(7587): 484–489.
- Silver, D.; Schrittwieser, J.; Simonyan, K.; Antonoglou, I.; Huang, A.; Guez, A.; Hubert, T.; Baker, L.; Lai, M.; Bolton, A.; et al. 2017. Mastering the game of go without human knowledge. *Nature* 550(7676): 354–359.
- Smith, E. R.; and Zarate, M. A. 1992. Exemplar-based model of social judgment. *Psychological review* 99(1): 3.
- Son, K.; Kim, D.; Kang, W. J.; Hostallero, D. E.; and Yi, Y. 2019. Qtran: Learning to factorize with transformation for cooperative multi-agent reinforcement learning. In *ICML*.
- Sukhbaatar, S.; Fergus, R.; et al. 2016. Learning multiagent communication with backpropagation. In *NeurIPS*.
- Sunehag, P.; Lever, G.; Gruslys, A.; Czarnecki, W. M.; Zambaldi, V. F.; Jaderberg, M.; Lanctot, M.; Sonnerat, N.; Leibo, J. Z.; Tuyls, K.; et al. 2018. Value-Decomposition Networks For Cooperative Multi-Agent Learning Based On Team Reward. In *AAMAS*.
- Vinyals, O.; Babuschkin, I.; Czarnecki, W. M.; Mathieu, M.; Dudzik, A.; Chung, J.; Choi, D. H.; Powell, R.; Ewalds, T.; Georgiev, P.; et al. 2019. Grandmaster level in StarCraft II using multi-agent reinforcement learning. *Nature* 575(7782): 350–354.
- Zhang, K.; Yang, Z.; Liu, H.; Zhang, T.; and Başar, T. 2018. Fully decentralized multi-agent reinforcement learning with networked agents. *arXiv:1802.08757* .



## Additional Details on Push Experiments

Here we describe the specifications of networks and hyperparameters for training the compared methods in the experiments on *Push*.

For all the methods, the Q-network consists of 4 fully connected layers, with 128 hidden units and ReLU activation function in each layer.

For all the methods except DQN, the encoder network consists of a 2-layer LSTM with the concatenated history of a 50-timestep episode as the input, and an embedding layer that outputs 32-dimensional embeddings. DPIQN’s encoder has an additional prediction layer that outputs the predicted action for the opponent. The number of hidden units in each layer is 128. The output 32-dimensional embeddings are then feed to the Q-network where they are concatenated with the hidden state generated by the observation forwarded through the first fully connected layer of the Q-network. The concatenation is then forwarded through the rest 3 fully connected layers.

For training, the learning rate is set to  $1e-3$ , batch size is set to 64, and the discount factor is 0.99. In the IPR experiments, 200 episodes are collected for the initial random sampling of joint action distributions.

## Additional Details on Keep Experiments

Our implementation of PPO+IPR is modified based on PPO-Clip in *Spinning Up*, which have some difference in detail from Algorithm 1. The training process is described in Algorithm 2. PPO is an on-policy algorithm so that a large amount of samples are required. In order to sample more efficiently, we implement parallel rollouts for sampling. Calculating Wasserstain distance requires each sample set to be the same size, so we simplify the task setting by sampling with  $\mathcal{N}$  different opponent policies in parallel. Concretely, each opponent policy is assigned to  $M$  rollouts of length  $T$ . In other words, there are  $\mathcal{N}M$  rollouts in parallel, and we collect  $MT$  samples with each opponent policy (lines 3). Sliced Wasserstain distances are re-calculated every iteration in PPO+IPR-RS, while PPO+IPR-NoRS only uses sliced Wasserstain distances calculated at the first iteration (lines 4-6). The parameters of policy network and its IPR network are updated using the surrogate objective of PPO-Clip and  $\mathcal{L}_{\text{embed}}$ , respectively. The parameters of value function network and its IPR network are updated using the value function loss in PPO and  $\mathcal{L}_{\text{embed}}$ , respectively. We do not back-propagate the gradient from policy and value function to the IPR networks.

For all methods, we set  $\mathcal{N} = 4$ ,  $M = 2$ ,  $T = 1000$  and  $K = 3000$ . For PPO, both policy network and value network consist of 2 fully connected layers with 32 hidden units and Tanh activation function. For other methods, the encoder network consists of a LSTM layer and an embedding layer that outputs 32-dimensional embedding and optimized via truncated back-propagation through time with a truncation of 10 timesteps. PPO+ActPred has 2 additional fully connected layers that outputs the predicted action distribution for the opponent. Then the embedding is concatenated with the 32-dimensional hidden state generated by the observation forwarded through the first fully connected layer. The

## Algorithm 2 Joint Training of IPR and PPO

---

**Require:** Training policy set  $\Pi_o^{\text{train}} = \{\pi_o^1, \pi_o^2, \dots, \pi_o^{\mathcal{N}}\}$

- 1: Initialize  $\mathcal{E}$ , policy parameters  $\vartheta_\pi$ , value function parameters  $\vartheta_v$ , IPR network parameters  $\theta_\pi$  for policy and  $\theta_v$  for value function
- 2: **for** iteration  $k = 0, 1, \dots, K$  **do**
- 3:   Collect sets of trajectories  $\mathcal{D}_1, \mathcal{D}_2, \dots, \mathcal{D}_{\mathcal{N}}$  with all training policies in parallel.
- 4:   **if** IPR-RS **or**  $k == 0$  **then**
- 5:     Calculate  $d(\pi_o^i, \pi_o^j)$  for all  $(i, j)$  using  $\mathcal{D}_i, \mathcal{D}_j$
- 6:   **end if**
- 7:   Update  $\theta_\pi$  and  $\vartheta_\pi$  by  $\mathcal{L}_{\text{embed}}(\theta_\pi) + \mathcal{L}_{\text{CLIP}}(\vartheta_\pi)$
- 8:   Update  $\theta_v$  and  $\vartheta_v$  by  $\mathcal{L}_{\text{embed}}(\theta_v) + \mathcal{L}_V(\vartheta_v)$
- 9: **end for**

---

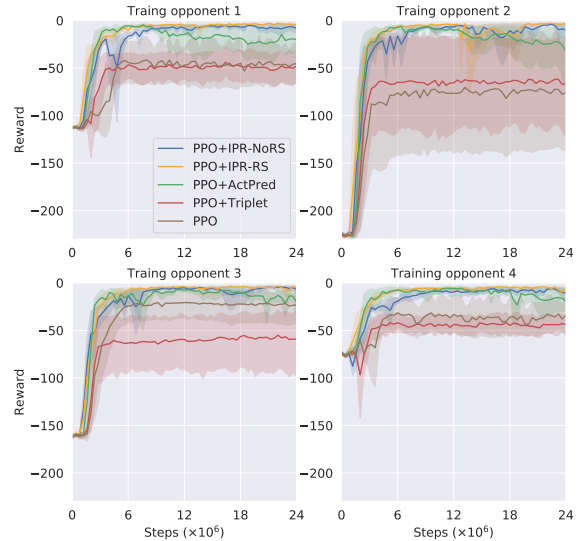


Figure 10: Learning curves on *Keep*. The four charts shows average rewards against different training opponent policies. At each checkpoint, rewards are averaged on 100 episodes. Each curve corresponds to the mean value of 5 trials with different random seeds, and shaded regions indicate 95% CI.

concatenation is then forwarded through the rest 2 fully connected layers with 32 hidden units and Tanh activation function. Other hyperparameters are the same as the default settings in *Spinning Up*.

## Experimental Results Against Training Opponent Policies

The learning curves of the compared methods against training opponent policies on *Keep* are shown in Figure 10. The result suggests that PPO+IPR-NoRS, PPO+IPR-RS and PPO+ActPred outperform PPO+Triplet and PPO significantly on training set. The curves of the former three methods on training set are close, but we can see PPO+IPR-NoRS and PPO+IPR-RS show less variance and keep reward high and stable in the later stage of training. On *Push*, the learning curves of the compared methods against training opponent policies are similar and close, thus omitted.